Optical Materials 60 (2016) 618–626

Contents lists available at ScienceDirect

Optical Materials

journal homepage: www.elsevier.com/locate/optmat

The basic spectroscopic parameters of Ho^{3+}-doped fluoroindate glass for emission at 3.9 μm

Laercio Gomes [a], Vincent Fortin [b], Martin Bernier [b], Réal Vallée [b], Samuel Poulain [c], Marcel Poulain [c], Stuart D. Jackson [d, *]

[a] Center for Lasers and Applications, IPEN/CNEN-SP, P.O. Box 11049, São Paulo, SP, 05422-970, Brazil
[b] Center for Optics, Photonics and Lasers (COPL), Université Laval, Québec, G1V 0A6, Canada
[c] Le Verre Fluoré, Campus KerLann, F-35170, Bruz, Brittany, France
[d] MQ Photonics, Department of Engineering, Faculty of Science and Engineering, Macquarie University, North Ryde, 2109, Australia

ARTICLE INFO

Article history:
Received 16 June 2016
Received in revised form
1 August 2016
Accepted 22 August 2016
Available online 30 September 2016

Keywords:
Spectroscopy of laser materials
Fluoride glass
Fibre lasers
Mid-infrared

ABSTRACT

This report details the first study of the fundamental spectroscopic properties of a new optical material for prospective application as a gain medium for fiber laser emission at 3.9 μm. We have investigated the decay processes that are relevant to the excited states of the $^5I_5 \rightarrow {}^5I_6$ transition in singly Ho^{3+}-doped InF_3 (fluoroindate) glass using time-resolved fluorescence spectroscopy. The HoF_3 concentration in the glass was 10 mol.%. We excited the $^5I_7$ and $^5I_6$ energy levels using selective excitation at 1982 nm and 1150 nm, respectively. We have established that a strong energy-transfer upconversion process by way of the well-known dipole-dipole interaction between two holmium ions excited to the $^5I_6$ level populate the $^5I_5$ (upper laser) level of the 3.9 μm transition. The $^5I_6$ and $^5I_5$ energy levels emit luminescence with measured peaks located at 2.85 μm and 3.92 μm, respectively and the luminescence efficiencies of these emissions are 78% and 0.2%, respectively. Results from numerical simulations show that for this high Ho^{3+} concentration, a population inversion for the 3.9 μm transition is reached only for a short time ($t < 100$ μs) after direct upper laser level pumping at a wavelength of 889 nm.

© 2016 Elsevier B.V. All rights reserved.

1. Introduction

Powerful and highly efficient fiber lasers with emission at wavelengths longer than 3 μm are needed for applications in sensing, nonlinear optics, frequency combs, materials processing and optical pumping. Since the first demonstration of longest emission wavelength from a fiber laser at 3.9 μm two decades ago [1,2], the only extension of this pioneering work was the recent demonstration of pulsed emission from a bulk InF_3 sample pumped by Cr^{3+}:LiSAF laser emitting at 889 nm [3] and the demonstration of supercontinuum generation using InF_3-based fibre [4]. Whilst a number of transitions at intermediate wavelengths between this limit and 3 μm have recently produced more than 1 W CW from a fiber laser [5,6], more work is clearly required to address the limited number of fiber lasers emitting at longer wavelengths. All the major demonstrations of mid-infrared emission from fiber lasers have employed fibers made primarily from fluorozirconate glass, limiting the operation at 3.9 μm to cryogenic temperatures. Fluoroindate glasses were discovered by M. Poulain in 1981 and display a lower phonon energy than ZBLAN which shifts multiphonon absorption edge by approximately 1 μm InF_3 glasses are 15 times more transparent at 3900 nm than ZBLAN glasses. The main components of those glasses are InF_3, SrF_2, BaF_2 and ZnF_2.

In this report, we investigate the luminescence and energy level decay properties of Ho^{3+}-doped fluoroindate glass. We carry out the basic spectroscopic measurements, compare the results with other previously reported fluoroindate glasses and assess the suitability of this optical material for emission in the mid-infrared. We calculated the luminescence efficiency of these levels after the experimentally determined decay time characteristics were compared with the calculated radiative lifetimes from Judd-Ofelt theory. Multiphonon decay and cross-relaxation resulted in the rapid depopulation of the $^5F_5$ and $^5I_5$ energy levels to the two lower excited states, namely the $^5I_6$ and $^5I_7$ levels. A numerical model is used to understand the gain dynamics of the $^5I_5 \rightarrow {}^5I_6$ transition in singly Ho^{3+}-doped InF_3 fluoroindate glass for comparatively high Ho^{3+} concentration.

* Corresponding author.
E-mail address: stuart.jackson@mq.edu.au (S.D. Jackson).

http://dx.doi.org/10.1016/j.optmat.2016.08.019
0925-3467/© 2016 Elsevier B.V. All rights reserved.

2. Experimental procedure

For this preliminary study, we prepared one fluoroindate (In Sr Ba Zn Ho) glass sample that was doped with 10 mol%HoF_3. The sample was prepared from high purity raw materials with 99.99% pure InF_3, 99.99% pure SrF_2, 99,99% pure BaF_2, 99.9% pure ZnF_2, 99.99% pure HoF_3. The precursor materials were melted in a Pt-Au crucible that was placed in a dry glove box environment at 820 °C for 60 min. This procedure reduced the water (OH) content in the glass. The glass liquids were decanted into brass molds that were polished and annealed at 300 °C for 1 h to remove any mechanical stresses. The sample was then cut and polished into $5.3 \times 5.3 \times 20$ mm^3 rectangular prism. The Ho^{3+} ion density in the sample was calculated to be 2×10^{21} cm^{-3} for the doped InF_3 sample with 10 mol. % HoF_3, respectively.

The absorption spectra of the glass sample (in the range between 2 μm and 10 μm) was measured using a Nicolet 6700 FTIR spectrophotometer. A tunable optical parametric oscillator (OPO) was used to measure the decay characteristics of the excited levels; the pulse characteristics were 10 mJ, 4 ns, and 10 Hz for most of the experiments. The OPO was tuned to 645 nm, 889 nm, 1150 nm and 1982 nm, in order to excite the $^5F_5$, $^5I_5$, $^5I_6$ and $^5I_7$ energy levels, respectively. A Judson model J-10 D InSb infrared detector (cooled to 77 K) was used to detect the infrared luminescence (for $\lambda > 1080$ nm). A fast preamplifier (response time approximately 0.5 μs) was used to amplify the signal. A photomultiplier tube (EMI, response time 10 ns) was employed to detect the visible and near infrared (i.e., $\lambda < 1100$ nm) luminescence. All measurements were carried out at 300 K. Bandpass filters each with ~80% transmission at 1200, 2100 and 4000 nm with a half width of 25 nm and an extinction coefficient of approximately 10^{-5} outside this band were used to separate the infrared luminescence.

3. Experimental results

When Ho^{3+}-doped fluoroindate glass is excited at 889 nm, the main processes involving the energy levels are, see Fig. 1: (*a*) ground state absorption (GSA), $^5I_8 + h\nu(889\ nm) \rightarrow Ho^{3+5}I_5$; (*b*) non-radiative multiphonon decay (NR), $^5I_5 \rightarrow {}^5I_6 + p\hbar\omega$ ($p = 5$); (*c*) energy transfer upconversion (ETU_1), $^5I_7 + {}^5I_7 \rightarrow {}^5I_6 + {}^5I_8 + p\hbar\omega$ ($p \sim 3$); (*d*) energy transfer upconversion (ETU_2), $^5I_6 + {}^5I_6 \rightarrow {}^5F_5 + {}^5I_8 + p\hbar\omega$ ($p \sim 3$) and (e) cross-relaxation (CR), $^5I_5 + {}^5I_8 \rightarrow {}^5I_7 + {}^5I_7$. The term $\hbar\omega$ relates to the phonon energy of the glass.

The absorption spectrum of the Ho^{3+} ion when doped into InF_3 glass was measured in the near and mid-infrared regions of the spectrum using a Cary 5000 and the FTIR Nicolet spectrophotometers each operating in transmission mode. The measured absorption spectrum of the electronic transitions for Ho(10%)-doped InF_3 glass is shown by Fig. 2(a). The absorption coefficient (cm^{-1}) was measured using $\alpha = 2.303 \times O.D./d$, where O.D. is the optical density and d is the sample length which was equal to 5.2 mm. The absorption cross-sections for the sample were calculated using the well-known relation $\alpha = \sigma_{abs}/N_{Ho}$, where $N_{Ho} = 2 \times 10^{21}$ cm^{-3} (for a 10 mol%concentration). The cross section values were: $\sigma_{abs} = 4.86 \times 10^{-21}$ cm^2 (for $\lambda = 1945$ nm), 2.35×10^{-21} cm^2 (for $\lambda = 1150$ nm) and 4.3×10^{-22} cm^2 (for $\lambda = 889$ nm) relating to the peak of the $^5I_8 \rightarrow {}^5I_7$, $^5I_6$, and $^5I_5$ transitions, respectively. Fig. 2(b) shows the mid-infrared absorption of Ho^{3+}(10%)-doped InF_3 glass exhibiting the absorption from OH^- free radicals with a wavenumber peak at 3160 cm^{-1} (or 3165 nm). The OH^- group absorption in glasses depends on the glass composition and is associated with hydrogen bonding that couples to the network former cation, such as the In^{3+} ion in the present study. Thus, the difference between OH^- group absorption peaks is the strength of the hydrogen-cation association; a stronger association will shift the OH^- absorption peak to longer wavelength. For example, in silicate glasses the OH^- group has absorption peak located at 3550 cm^{-1} while in germanotellurite glasses it has an absorption peak closer to 3000 cm^{-1}.

The absorption coefficient was determined to be $\alpha = 0.060$ cm^{-1}. The OH^- group concentration can be calculated using the relation $N_{OH} = N/\varepsilon\alpha$, where N is the Avogadro constant, and ε is the molar absorptivity of the OH^- groups in the glass. We assumed the parameter ε was 49.1×10^3 cm^2/mol [7], which gave a value for N_{OH} of 7.4×10^{17} cm^{-3} for the sample.

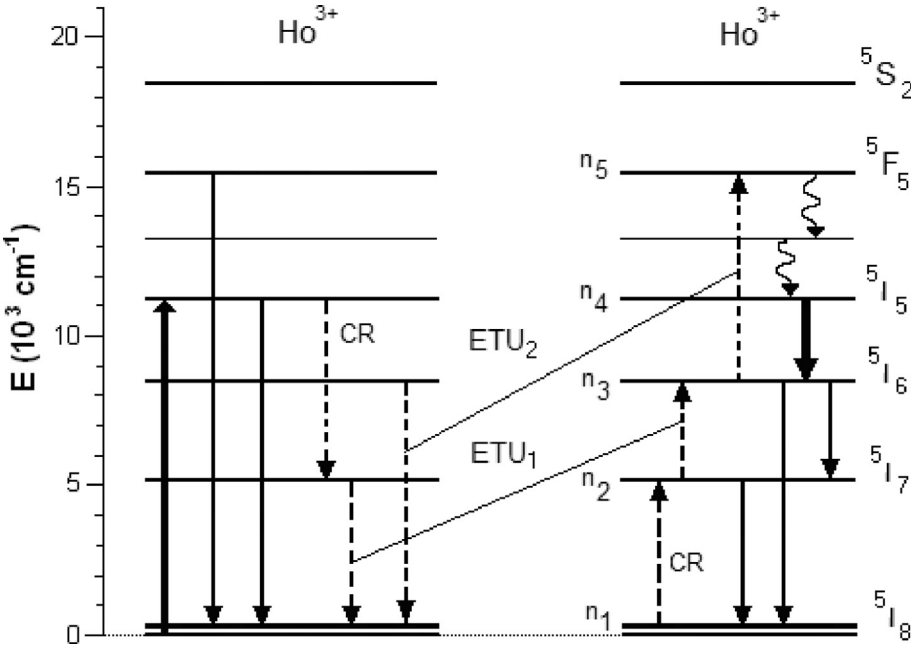

Fig. 1. Energy level scheme showing the pump, laser energy transfer mechanisms relevant to the laser operation at 3.9 μm. Solid line (up): 889 nm excitation. Solid lines (down): Ho^{3+} emissions (at 645, 889, 1163, 2026, 2860 and 3930 nm). Dashed lines (up and down): ETU_1, ETU_2 and CR processes.

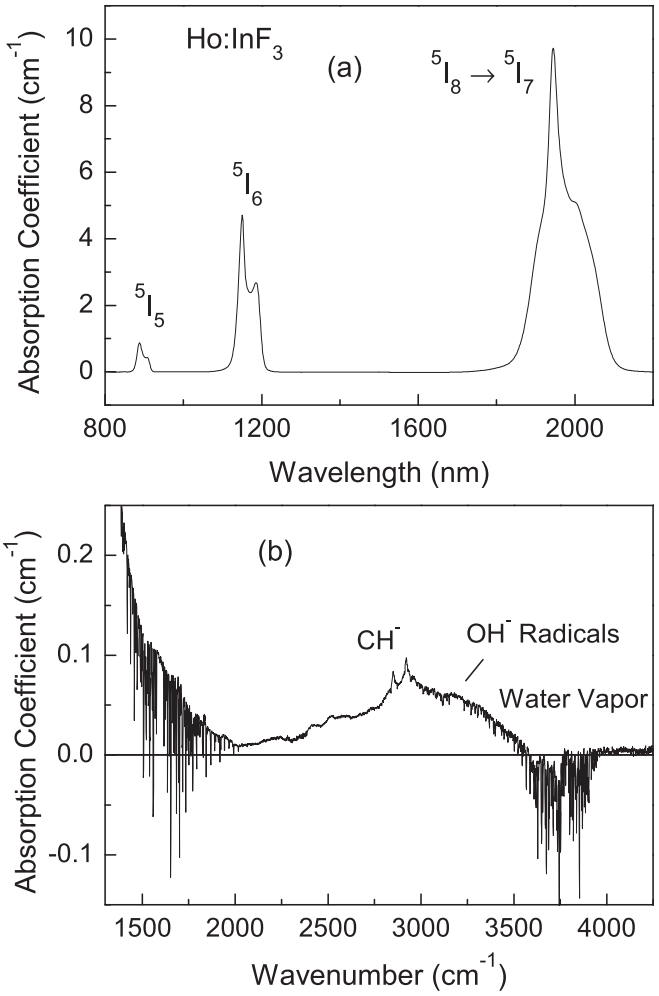

Fig. 2. Measured absorption spectrum in (a) the near infrared region and (b) the mid-infrared region using the FTIR Nicolet spectrophotometer (in transmission mode). The optical length of the sample was d = 5.2 mm.

In the Judd-Ofelt calculation, the rate of spontaneous emission from an excited state of a rare earth ion (in the 3 + ionised state) ion that results from an electric dipole transition between J and J' is determined by Eq. (1)

$$A^{ed}(J,J') = \frac{64\pi^4}{3h}\frac{1}{(2J+1)\bar{\lambda}^3}\left[\frac{n(n^2+2)^2}{9}\right]S^{ed}, \quad (1)$$

where $S^{ed} = e^2 \sum_{\lambda=2,4,6} \Omega_\lambda \left|\langle U^{(\lambda)}\rangle\right|^2$. The spectroscopic intensity parameters Ω_2, Ω_4 and Ω_6 are equal to 1×10^{-20} cm^2, 2.8×10^{-20} cm^2 and 1.9×10^{-20} cm^2, respectively for Ho^{3+}-doped fluoroindate glass [8]. Values of $\left|\langle U^{(\lambda)}\rangle\right|^2$ were obtained from the literature [9] for the radiative transitions of Ho^{3+} in LaF_3 (aquo ions). The refractive index used in the calculation was $n = 1.49$ for InF_3. Table 1 shows the calculated values of the radiative rates ($A_{JJ'}$) and radiative lifetimes (τ_R) calculated using Judd-Ofelt theory for some of the relevant luminescence emitting transitions.

3.1. Emission spectrum of the $^5I_5$, $^5I_6$ and $^5I_7$ levels

The emission spectrum from the Ho^{3+}-doped sample was obtained using a scanning monochromator (KRATOS) in conjunction with the InSb detector and a Box-Car averager. The emission cross section due to the $^5I_5 \rightarrow {}^5I_6$ (see Fig. 3), $^5I_6 \rightarrow {}^5I_7$ (see Fig. 4) and $^5I_7 \rightarrow {}^5I_8$ (see Fig. 5) transitions was calculated using

$$\sigma_{emis}(\lambda) = \frac{\bar{\lambda}^4}{8\pi n^2 c} A_{ij} \frac{I(\lambda)}{\int I(\lambda) d\lambda}, \quad (2)$$

where $\bar{\lambda}$ is the average emission wavelength or centroid, A_{ij} (s^{-1}) is the radiative transition probability, S(λ) is the line shape of the emission band, $\int I(\lambda)\, d\lambda$ is the integrated line shape, n is the refractive index (1.49) and c is the speed of light. $\varepsilon(\bar{\lambda}) = \frac{I(\bar{\lambda})}{\int I(\lambda)\, d\lambda}$ is the normalized line shape at the emission wavelength at the barycenter($\bar{\lambda}$). Equation (2) is based on the Füchtbauer–Ladenburg equation i.e., $\sigma_{21}(\lambda) = \frac{\lambda_0^4}{8\pi c n^2} A_{21}\, g_{21}(\lambda)$, where the lineshape $g_{21}(\lambda)$ is normalized, i.e., $\int g_{21}(\lambda)\, d\lambda = 1$ and c is the speed of light in vacuum and λ_0 is the center wavelength of the 2 → 1 electronic transition. Electronic transitions in the glass form a broad band due to the

Table 1
Radiative rates and radiative lifetime calculated using Judd-Ofelt theory for Ho^{3+} in InF_3 glass.

Radiative transition	Wavelength λ (nm) (barycenter)	Radiative rate ($A_{JJ'}$) (s^{-1})	Radiative lifetime τ_R (ms)
$^5F_5$ →			0.321
$^5I_5$	2275	12	
$^5I_6$	1438	145	
$^5I_7$	960	598	
$^5I_8$	645	2360	
$^5I_5$ →			6.8
$^5I_6$	3930	2	
$^5I_7$	1640	63	
$^5I_8$	889	81	
$^5I_6$ →			6.2
$^5I_7$	2860	11	
$^5I_8$	1163	150	
$^5I_7$ →			16.2
$^5I_8$	2026	62	

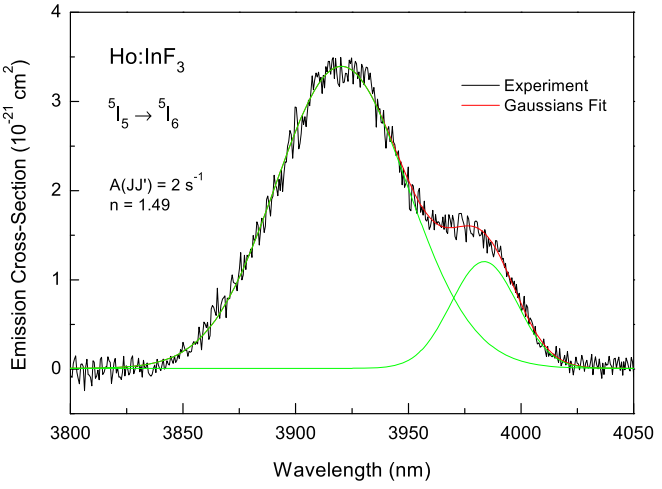

Fig. 3. Emission spectrum of the $^5I_5 \rightarrow {}^5I_6$ transition using laser excitation at 890 nm (E = 11 mJ). The emission cross-section was calculated using $\bar{\lambda} = 3930$ nm, $A_{ij} = 2\ s^{-1}$ and $\varepsilon(\bar{\lambda}) = 0.011367\ nm^{-1}$. A two Gaussians best fit (red lines) shows peaks p_1 at 3920 nm ($w_1 = 58$ nm) and p_2 at 3984 nm ($w_2 = 30$ nm). (For interpretation of the references to colour in this figure legend, the reader is referred to the web version of this article.)

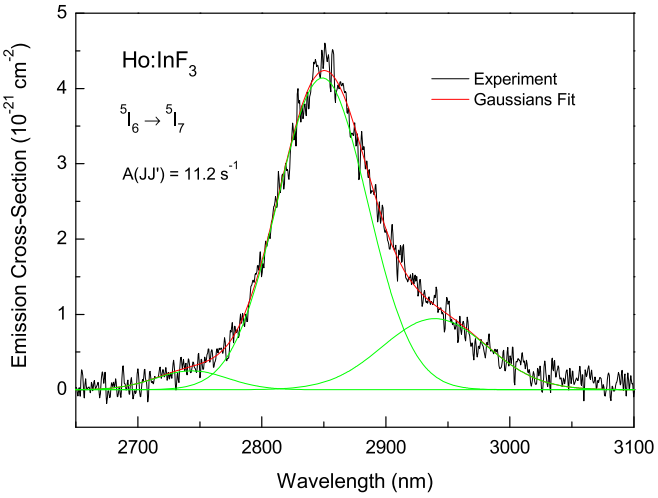

Fig. 4. Emission spectrum of $^5I_6 \rightarrow {}^5I_7$ transition using a laser excitation at 890 nm (E = 11 mJ). The emission cross-section was calculated using $\bar{\lambda}$ = 2860 nm, A_{ij} = 11.2 s^{-1} and $\varepsilon(\bar{\lambda})$ = 0.008753 nm^{-1}. A three Gaussians best fit (red lines) shows peaks p_1 at 2743 nm (w_1 = 58 nm), p_2 at 2849 nm (w_2 = 72.4 nm) and p_3 at 2939 nm (w_3 = 85 nm). (For interpretation of the references to colour in this figure legend, the reader is referred to the web version of this article.)

multiple Ho^{3+} ion sites present in the host glass and that the emission is asymmetric because of the different kind of site symmetries (or groups), we propose that the center wavelength λ_0 (which is the peak position for a narrow emission band) should be replaced by the average wavelength. The wavelength is therefore better represented by the emission band centroid. The $^5I_5 \rightarrow {}^5I_6$, $^5I_5 \rightarrow {}^5I_7$ and $^5I_5 \rightarrow {}^5I_8$ emission bands were decomposed into in two or three Gaussian curves that suggested that the Ho^{3+} ions are preferentially located in two (or three) different types of sites symmetries (or groups) in the glass.

3.2. Luminescence decay of the $^5I_7$ and $^5I_6$ levels

When the sample was excited at 1150 nm (i.e., directly

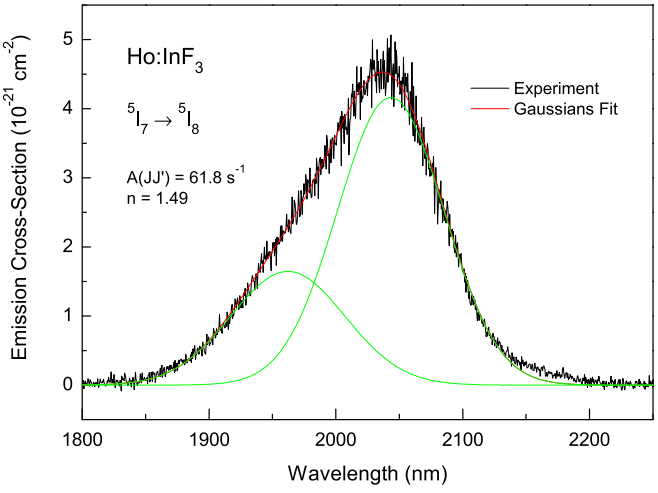

Fig. 5. Emission spectrum of $^5I_7 \rightarrow {}^5I_8$ transition using a laser excitation at 890 nm (E = 11 mJ). The emission cross-section was calculated using $\bar{\lambda}$ = 2026 nm, A_{ij} = 61.8 s^{-1} and $\varepsilon(\bar{\lambda})$ = 0.00706 nm^{-1}. A two Gaussian function best fit (red lines) shows peaks p_1 at 1962 nm (w_1 = 90 nm) and p_2 at 2043 nm (w_2 = 84 nm). (For interpretation of the references to colour in this figure legend, the reader is referred to the web version of this article.)

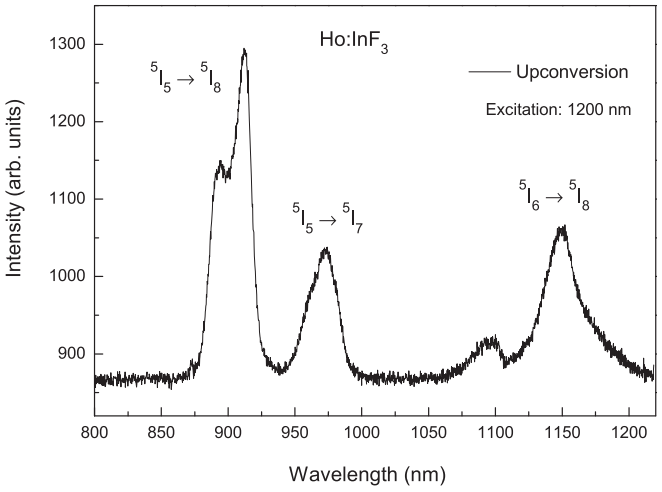

Fig. 6. Measured upconversion luminescence spectrum after laser excitation of the $^5I_8 \rightarrow {}^5I_6$ transition at 1200 nm.

populating the $^5I_6$ level), the upconversion luminescence at 645 nm from the $^5F_5$ excited state of Ho^{3+} is observed due to ETU_2 (see Fig. 6). Laser excitation at 1982 nm (to directly excite the $^5I_7$ level) did not produce visible upconversion luminescence using < 11 mJ probe pulses. The best fit to the temporal decay characteristics relevant to the $^5I_6$ and $^5I_7$ energy level decay characteristics were accurately described by the experimental decay function

$$I(t) = I_0 \exp\left(-\gamma\sqrt{t} - \frac{t}{\tau_d} - \overline{W}\, t \right), \tag{3}$$

where $\tau_d = \tau_R/1+W_{NR}\,\tau_R$ is the intrinsic decay of donor, τ_R is the radiative decay of the donor and W_{NR} is the multiphonon decay rate. The non-exponential term $\exp(-\gamma\sqrt{t})$, i.e., the classical Förster decay function, describes energy transfer processes (donor → acceptor) without energy migration through donor states. This process is also known as static disordered decay involving the dipole-dipole interaction [10]. The parameter γ ($s^{-1/2}$) is the energy transfer parameter. The term $\exp(-\overline{W}\, t)$ in Eq. (3) describes energy transfer (donor → acceptor) processes that are enhanced by energy migration, typically explained using Burshtein's hopping model [11] in which the excited-state population

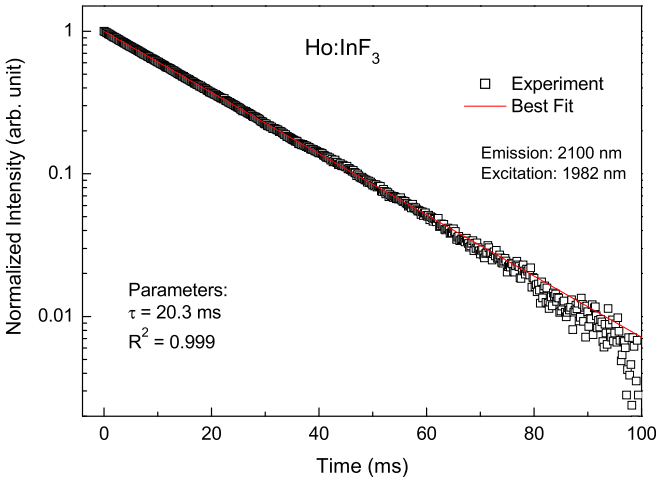

Fig. 7. Emission decay curve measured at 2100 nm ($^5I_7 \rightarrow {}^5I_8$) after laser excitation at 1982 nm.

redistributes randomly over donors at a characteristic hopping rate $1/\tau_0$. Burshtein established that donor excitation always decays exponentially at long times in both weak and strong excitation migration [11,12]. Considering a non-exponential decay of the donor, the mean decay time (τ) of the donor excitation can be obtained by the integration of the decay curve (Eq. (3)) using

$$\tau = \frac{1}{I_0}\int_0^\infty I(t)dt. \quad (4)$$

Thus, the exponential and non-radiative components of the fluorescence decay are combined into the one parameter i.e., τ. Eq. (3) describes the two asymptotic cases of the donor excitation decay: i) non-exponential decay at short times when $t << \tau$ and ii) the exponential decay at longer times (or $t >> \tau$). Eq. (3) has been used to describe the luminescence self-quenching of Tm^{3+} in $YLiF_4$ crystals due to cross-relaxation process for low (0.5 mol%) and high (5 and 10 mol.%) concentration of Tm^{3+} [13].

Eq. (3) was rewritten in order to show the fitting parameters, t_1 and γ giving

$$I(t) = \exp\left(-\gamma\sqrt{t} - \frac{t}{t_1}\right), \quad (5)$$

where $t_1 = \frac{\tau_d}{1+\tau_d W}$. The best-fit parameters and the integrated lifetime are i) $\gamma = 0$ and $t_1 = 20.3$ ms ($R^2 = 0.9999$) ($\tau = \tau_d = t_1$) for the $^5I_7$ level, and ii) $\gamma = 0$ and $t_1 = 4.8$ ms ($R^2 = 0.9998$) ($\tau = \tau_d = t_1$) for the $^5I_6$ level. The experimental decay curves are shown in Figs. 7 and 8.

We observed that the $^5I_6$ excited level decay in Ho(10%):InF_3 glass has a decay time of 4.8 ms which is close to the radiative lifetime of 6.2 ms. We conclude therefore that only a small multiphonon decay (rate of 47 s^{-1}) is competing with the radiative decay. The excitation energy was kept low enough (i.e., E ~6 mJ) to avoid the up-conversion which might introduce a decrease in the decay time at higher excitation energies. The weak overlap between the $^5I_6 \rightarrow {}^5I_8$ emission band of Ho^{3+} (peak at 2860 nm) and the OH^- group absorption (peak at 3165 nm) should produce minimal energy transfer to OH^- radicals in InF_3 glass due to the strong hydrogen-cation former association that shifts the absorption peak to longer wavelength. In addition, the relatively low concentration of OH^- radicals (of 7.4×10^{17} cm^{-3}) determined for this sample also helped to keep the $^5I_6$ level decay time (of 4.8 ms) close to the radiative value of 6.2 ms. The decay time of $^5I_7$ level was observed to be 20.3 ms (Fig. 7), which is longer than the radiative lifetime of 16.2 ms. The apparently extended decay time is attributed to excitation migration through the $^5I_7$ levels which is dependent on the Ho^{3+} concentration. The effective lifetime of this level is still considered to be $\tau_R = 16.2$ ms.

3.3. Luminescence decay from the $^5F_5$ and $^5I_5$ levels

Figs. 9 and 10 show the measured luminescence decay from the $^5F_5$ and $^5I_5$ levels after laser excitation at 644 nm and 890 nm, respectively. The best fit to the decay was accomplished using Eq. (5). The best-fit parameters and the integrated decay time are i) $\gamma = 0$ and $t_1 = 16.3$ μs ($R^2 = 0.9998$) ($\tau = \tau_d = t_1$) for the $^5F_5$ level, and ii) $\gamma = 350$ $s^{-1/2}$ and $t_1 = 135$ μs (intrinsic) ($R^2 = 0.9968$) for the $^5I_5$ level giving a total (integrated) decay time of the $^5I_5$ level of $\tau = 13$ μs We found that $\gamma = 0$ gave the best fit for the decay of the $^5F_5$ level, which indicates that cross-relaxation was not involved, however, the higher value of the γ parameter (= 350 $s^{-1/2}$) found for the $^5I_5$ level decay indicates that a strong cross-relaxation process (which we label CR_1) has introduced a strong non-exponential component to the decay time.

3.4. Non-radiative multiphonon decay

The non-radiative decay rate can be calculated using the decay time obtained from the best fit calculations and using the parameter W_{NR} (s^{-1}) = $1/\tau_d - 1/\tau_R$, where τ_d is the intrinsic decay time (without energy transfer). τ_R is the radiative lifetime calculated from Judd-Ofelt theory (see Table 1). The intrinsic decay constant τ_d is equal to the value of parameter t_1 obtained from best fit to the decay characteristic of the $^5I_7$ (see Fig. 7), $^5I_6$ (see Fig. 8), $^5F_5$ (see Fig. 9) and $^5I_5$ (see Fig. 10) levels. The intrinsic luminescence efficiency was calculated using $\eta_\ell = \frac{\tau}{\tau_R}$. Table 2 shows the resulting luminescence decay parameters. It is important to note that the luminescence decay from the $^5F_5$ level is fully exponential ($\gamma = 0$) which is a strong indication that multiphonon decay competes with radiative decay decreasing the decay time from 321 μs (i.e., the radiative lifetime) to 16.3 μs.

3.5. Energy transfer upconversion from the $^5I_7$ excited level

A study of the ETU_1 process was proceeded using the 1200 nm

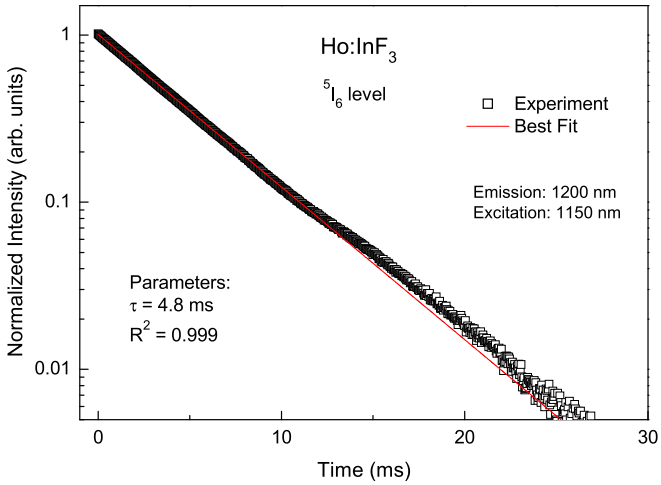

Fig. 8. Emission decay curve measured at 1200 nm ($^5I_6 \rightarrow {}^5I_8$) after laser excitation at 1150 nm.

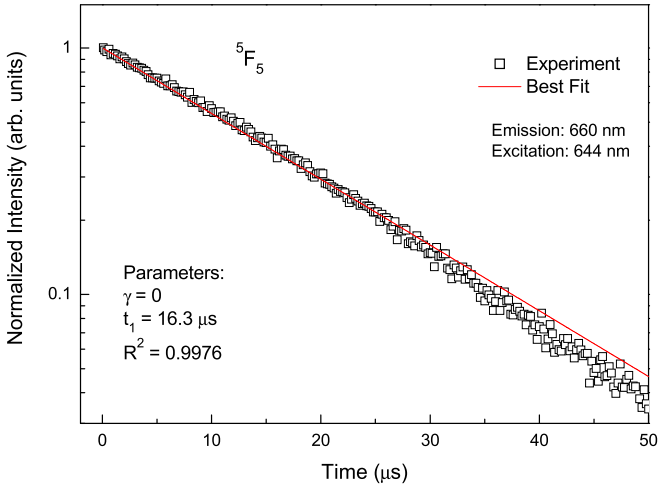

Fig. 9. Measured luminescence decay curve measured at 660 nm ($^5F_5 \rightarrow {}^5I_8$) after a pulse laser excitation at 644 nm.

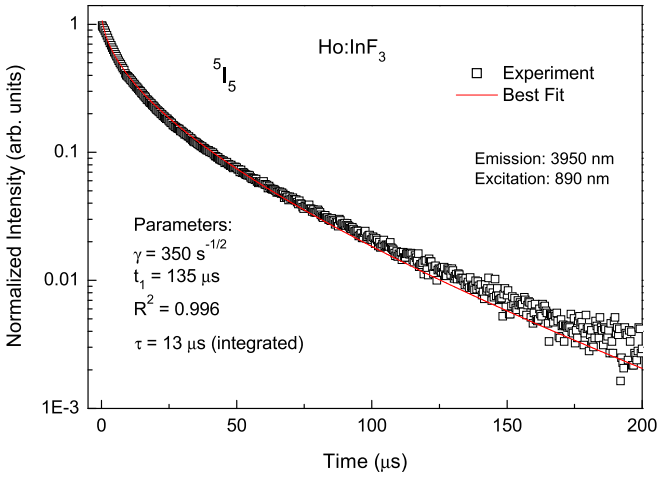

Fig. 10. Luminescence decay curve measured at 3950 nm ($^5I_5 \rightarrow {}^5I_6$) after a pulse laser excitation at 890 nm.

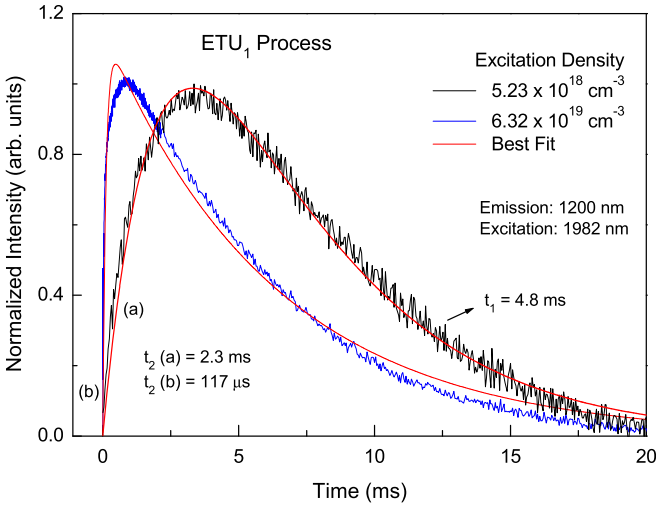

Fig. 11. Measured upconversion luminescence transient ($^5I_6$ level) measured at 1200 nm for laser pulse excitation at 1982 nm. The pulse duration was 4 ns (at 10 Hz) for these experiments and at lower excitation density the pulse energy was 8.6 mJ and the spot size was 0.0316 cm^2, for the higher excitation density the pulse energy was 13 mJ and the spot size was 0.00395 cm^2. The best-fit calculations are shown in red. (For interpretation of the references to colour in this figure legend, the reader is referred to the web version of this article.)

emission (from the $^5I_6$ level) produced by excitation of the $^5I_7$ energy level at 1982 nm. Fig. 11 shows the luminescence time transient measured for two excitation densities. One can observe that the transient rise time (t_2) decreases for higher excitation densities. The best-fit calculations were obtained using Eq. (6) [14].

$$I(t) = I_0\left[\exp\left(-\gamma_1\sqrt{t} - t/t_1\right) - \exp(-t/t_2)\right], \quad (6)$$

where I_0 is the amplitude of the ETU process. t_2 gives the risetime and t_1 the decay time of the luminescence transient. There are two cases to be considered: 1) γ_1, t_1 are the parameters for the acceptor decay and t_2 parameter for the upconversion when $\tau_{Up} < \tau_A$, and 2) γ_1, t_1 parameters are used for the upconversion and t_2 are gives the acceptor decay when $\tau_{Up} > \tau_A$. In the case of the $^5I_6$ level, γ_1 and t_1 parameters give the decay constant (4.8 ms) and t_2 gives the rise time of ETU_1. The best-fit parameters were found to be *i)* $\gamma_1 = 0$, $t_1 = 4.8$ ms and $t_2 = 2.3$ ms ($R^2 = 0.9879$) for the low excitation density ($N^* = 5.23 \times 10^{18}$ cm^{-3}) and *ii)* $\gamma_1 = 0$, $t_1 = 6.2$ ms, $t_2 = 117$ μs ($R^2 = 0.9878$) for the highest excitation density ($N^* = 6.23 \times 10^{19}$ cm^{-3}). The rise time (t_2) gives important information about the rate of ETU_1 because it is dependent on the excitation intensity and the increasing (by excitation migration) acceptor lifetime, t_1. ESA was not observed by way of visible light emission when the $^5I_7$ level was pumped. The rate probability (s^{-1}) for ETU_1 was obtained using $W_{ETU1} = 1/t_2 - 1/\tau_d$, where τ_d is the intrinsic lifetime of the $^5I_7$ level (donor) (see Table 2).

3.6. Critical radius model for ETU

Fig. 11 shows that the risetime (t_2) or ETU1 rate ($1/t_2$) of the $^5I_6$ excited level up-conversion luminescence is dependent on the excitation intensity. As can be observed in the results presented in Figs. 12 and 14, the ETU probability rate K increases with the increase in the Ho^{3+} excitation density (N^*) and reaches a constant value K_0 for $N^* > 1 \times 10^{19}$ ions cm^{-3}. The critical radius model, which has been presented previously in Ref. [15] explains this observation based on the existence of a critical radius R_C for the ETU interaction, which limits the ETU rate transfer to a constant value for all excited Ho - Ho pairs having a distance separation $R \leq R_C$. The average ETU efficiency $\eta_{ETU}(N^*)$ can be obtained by integrating the differential function $f\,dR$ that represents the random fraction distribution of two interacting Ho^{3+} excited ions within the distance R and R + dR and it is given by

$$f\,dR = 4\pi R^2 N_{Ho}\frac{N^*}{N_{Ho}}\left[1 - \frac{N^*}{N_{Ho}}\right]^{\left(\frac{4\pi}{3}R^3 N_{Ho} - 2\right)} dR,$$

where N^* is the density of excited Ho^{3+} (cm^{-3}) and N_{Ho} is the Ho^{3+} concentration in the sample. Assuming that those excited Ho^{3+} ions inside R_C will interact by way of ETU with efficiency $\eta = 1$. In contrast, those excited Ho^{3+} ions outside the R_C will not undergo ETU (i.e., $\eta = 0$). Applying this efficiency assumption to the $f\,dR$ distribution function and integrating ($\eta\, x\, f\, dR$) between R_m (minimal distance separation) and $R = \infty$, one obtains the overall ETU efficiency as a function of the excited Ho^{3+} concentration (cm^{-3})

$$\eta_{ETU} = \int_{R_m}^{R_C} f dR \times 1 + \int_{R_c}^{\infty} f\,dR \times 0 = 1 - \exp(-N^*/N_C). \quad (7)$$

where we use $\int_{R_C}^{\infty} f\,dR = \exp(-N^*/N_C)$ previously determined in

Table 2
Best fit luminescence parameters, non-radiative decay and cross-relaxation rates (s^{-1}).

Level	γ ($s^{-1/2}$)	τ(expt.) (ms)	τ_d (ms)	τ_R (ms)[a]	W_{NR} (s^{-1})	W_{CR} (s^{-1})	η_ℓ (%)
$^5F_5$	0	0.0163	0.0163	0.321	58234	0	0.42
$^5I_5$	350	0.013 (integrated)	0.135	6.8	7260	69231	0.20
$^5I_6$	0	4.8	6.2	6.2	47	0	77.5
$^5I_7$	0	20.3	16.2	16.2	0	0	100

[a] Radiative lifetimes (τ_R) were calculated from Judd-Ofelt theory in this work.

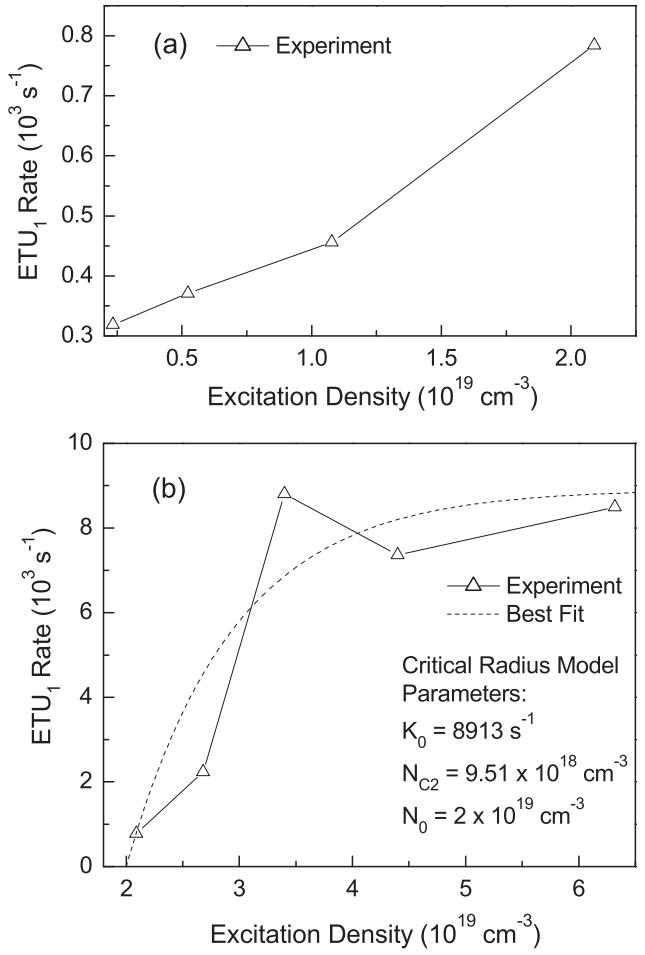

Fig. 12. Measured ETU_1 rate probability (s^{-1}) as a function of (a) low and (b) high excited Ho^{3+} ion density (N^*) obtained by measuring the luminescence transient from the $^5I_6$ level (at 1200 nm) after pulsed (4 ns) excitation at 1982 nm (triangles). The dashed line represents the best fit using the critical radius model.

Ref. [16]. The critical concentration N_C is related to the critical radius using $R_C^3 = 3/4\pi N_C$. The ETU rate K (s^{-1}) can be obtained from relation $K = K_0\ \eta$, where K_0 is the ETU rate constant obtained at

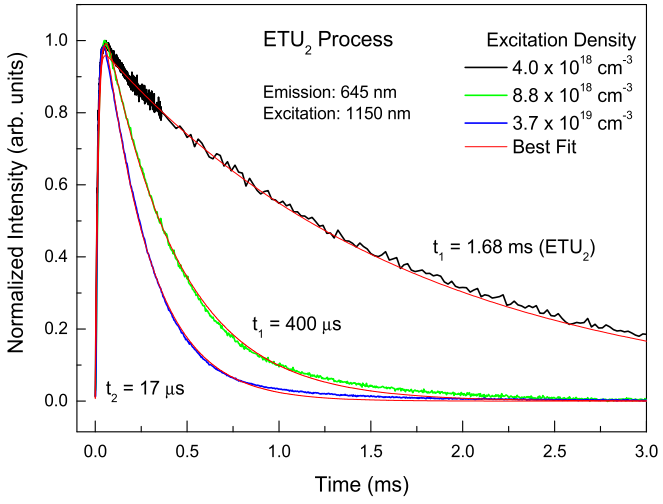

Fig. 13. Upconversion luminescence transient ($^5F_5$ level) measured at 645 nm under pulsed excitation at 1150 nm.

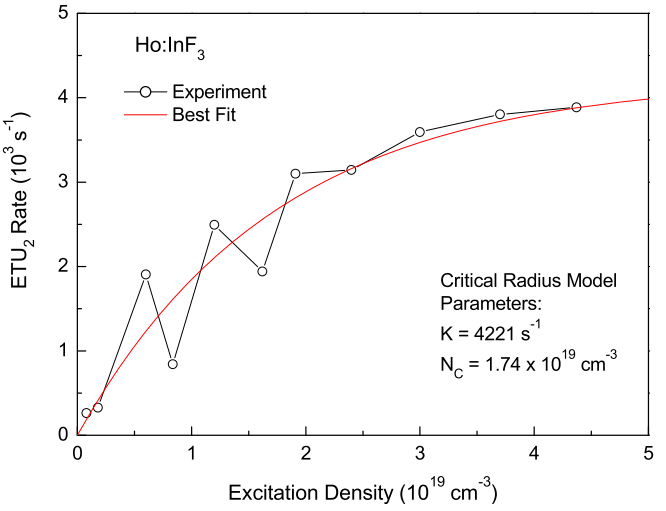

Fig. 14. Measured ETU_2 rate probability as a function of the excited Ho^{3+} ion density (N^*) after pulsed (4 ns) excitation at 1200 nm (open circles). The solid red line represents the best fit using the critical radius model using Eq. (7). (For interpretation of the references to colour in this figure legend, the reader is referred to the web version of this article.)

saturation where all the interacting ions are inside of the critical radius R_C. As a consequence of the model, K_0 is the constant rate for the excitation density $N^* > N_C \sim 1 \times 10^{19}$ cm^{-3}.

Fig. 12 shows the rate of K for ETU1 as a function of the excitation density after laser excitation at 1982 nm. In Fig. 12(b) one can observe that the rate of ETU_1 saturates to a value $K_0 = 8913$ s^{-1} found using Eq. (7). The results suggest that initially, see Fig. 12(a), the ETU_1 process is governed by a large critical radius interaction distance (R_{C1}) which is consistent with the linear dependence observed at low excitation densities, i.e., $N^* << N_C$ (where $\eta_{ETU} \approx N^*$). At higher excitation densities, see Fig. 12(b), the ETU_1 process can be described by a smaller critical radius interaction R_{C2} (= 20 Å) that forces the rate of ETU_1 to reach the saturated value for K_0. Note that the critical radius model has been applied with success to describe the ETU rate probability due to interacting $^4I_{13/2}$ excited states of Er^{3+}ions in fluoride glass [17–19].

3.7. Energy transfer upconversion from the $^5I_6$ excited level

Measurement of the 645 nm emission from the $^5F_5$ level after excitation of the $^5I_6$ energy level at 1150 nm allows an analysis of ETU_2. Fig. 13 shows the luminescence time transient measured for three excitation densities. One can observe a time dependent ETU_2, where the transient decay time (t_1) decreases for higher excitation densities. ETU_2 process dominates the emission properties of the 645 nm emission from the $^5F_5$ level and its decay time (t_1) becomes shorter as the excitation density increases above 1×10^{19} cm^{-3}. The best-fit curves in Fig. 13 were obtained using Eq. (6). In the case of the $^5F_5$ level, γ_1 and t_1 are the ETU_2 process parameters that are strongly affected by the excitation density and t_2 is the decay constant of $^5F_5$ level (17.5 µs) for Ho^{3+}-doped fluoroindate glass at 300 K. The best-fit parameters were *i)* $\gamma_1 = 0$, $t_1 = 1.68$ ms and $t_2 = 11$ µs ($R^2 = 0.9960$) for $N^* = 4 \times 10^{18}$ cm^{-3}, *ii)* $\gamma_1 = 0$, $t_1 = 400$ µs and $t_2 = 17.7$ µs ($R^2 = 0.9976$) for $N^* = 8.84 \times 10^{18}$ cm^{-3} and *iii)* $\gamma_1 = 0$, $t_1 = 252.3$ µs and $t_2 = 16.7$ µs ($R^2 = 0.9977$) for $N^* = 3.7 \times 10^{19}$ cm^{-3}. ESA was not observed for laser excitation tuned in the $^5I_8 \rightarrow {}^5I_6$ transition at 1150 nm.

The rate probability (s^{-1}) for ETU_2 was obtained using $W_{ETU2} = 1/t_1 - 1/\tau_d$, where τ_d is the intrinsic lifetime (= 4.8 ms) of the $^5I_6$ level (donor level) (see Table 2). Fig. 14 shows the values of

ETU2 rates (K) as a function of the excitation density. One can observe that the rate of ETU_2 tends to a constant value $K_0 = 4221$ s^{-1} according to the critical radius model used to fit the experimental data using Eq. (7). The ETU_2 process is governed by the critical interaction distance ($R_C = 24$ Å), which allows the rate of ETU_2 to stabilize to a value K_0 for $N^* > N_C = 1.74 \times 10^{19}$ cm^{-3}.

4. Rate equation modeling

Fig. 1 shows the basic energy level scheme for the Ho^{3+}-doped fluoroindate system. In our model we assume CW (or quasi-cw) excitation at 889 nm. In the model, the parameters n_1, n_2, n_3, n_4 and n_5 represent the populations in the $^5I_8$, $^5I_7$, $^5I_6$, $^5I_5$ and $^5F_5$ energy levels of Ho^{3+}, respectively. These levels are considered the most important and relevant to the laser transition at 3.92 μm (The $^5I_4$ level is strongly quenched by fast multiphonon decay.)

The rate equations for 889 nm pumping (assuming $n_1 + n_2 + n_3 + n_4 + n_5 = 1$) are.

$$\frac{dn_1}{dt} = -R_P\, n_1 + \frac{\beta_{51}}{\tau_{R5}} n_5 + \frac{\beta_{41}}{\tau_{R4}} n_4 + \frac{\beta_{31}}{\tau_{R3}} n_3 + \frac{\beta_{21}}{\tau_{R2}} n_2 + K_1 n_2^2 + K_2\, n_3^2 - W_{CR}\, n_1\, n_4 \quad (8)$$

$$\frac{dn_2}{dt} = \frac{\beta_{52}}{\tau_{R5}} n_5 + \frac{\beta_{42}}{\tau_{R4}} n_4 + \frac{\beta_{32}}{\tau_{R3}} n_3 - \frac{1}{\tau_{R2}} n_2 - 2\, K_1 n_2^2 + 2\, W_{CR}\, n_1\, n_4 + W_{NR}(32)\, n_3 \quad (9)$$

$$\frac{dn_3}{dt} = -\frac{n_3}{\tau_{R3}} - W_{NR}(32)\, n_3 + W_{NR}(43)\, n_4 + \frac{\beta_{43}}{\tau_{R4}} n_4 + \frac{\beta_{53}}{\tau_{R5}} n_5 + K_1\, n_2^2 - 2\, K_2\, n_3^2 \quad (10)$$

$$\frac{dn_4}{dt} = R_P\, n_1 - \frac{n_4}{\tau_{R4}} + W_{NR}(54)\, n_5 - W_{NR}(43)\, n_4 - W_{CR}\, n_1\, n_4 \quad (11)$$

$$\frac{dn_5}{dt} = -\frac{n_5}{\tau_{R5}} - W_{NR}(54)\, n_5 + K_2\, n_3^2 \quad (12)$$

where $R_P = \sigma_{14}\, I_P/h\nu_P$ is the pump rate (in s^{-1}), I_P is the pump light (in W cm^{-2}), and $h\nu_P$ is the photon energy of pump radiation. β_{ij} represents the luminescence branching ratio and τ_{Ri} is the radiative lifetime of excited states of Ho^{3+} labeled as $i = 2, 3, 4$ and 5. The absorption and emission cross-sections is $\sigma_{14} = 4.3 \times 10^{-22}$ cm^2 and $\sigma_{43} = 3.7 \times 10^{-21}$ cm^2 (at 3920 nm), respectively. All other parameters are given in Table 3.

Numerical solution of the rate equations was carried out to understand the potential for laser emission at 3.92 μm. The calculated evolution of the population inversion [(n_4-n_3), in mol.%] obtained by numerical simulation of the rate equations for [Ho^{3+}] = 10 mol.% using several pumping rates (R_P) from 100 to 2500 s^{-1} is shown in Fig. 15. The calculations show that a positive population inversion occurs only for a short time (t < 100 μs). At a longer pumping time (near t = 320 μs), the population n_3 and n_2 increases and the population inversion ($\Delta n = n_4 - n_3$) becomes strongly negative. The results presented in Fig. 15 show that the system cannot generate CW laser emission at 3.92 μm at the 10 mol.% concentration; laser emission can only be obtained for pulsed pumping with t_P < 100 μs This result is a direct consequence of the low intrinsic luminescence efficiency of 0.33% determined for the $^5I_5 \rightarrow {}^5I_6$ transition in fluoroindate glass. The low luminescence efficiency is a consequence of strong multiphonon decay and cross-relaxation at the current concentration level competing with radiative decay.

This result is in agreement with the experimentally observed laser characteristics for a similar glass reported in Ref. [3]. The best pump pulse duration is $t_P \approx 35$ μs with a repetition rate less than approximately 10 Hz in order to completely recover the ground state population. The results presented in Fig. 16 show that ETU_1 process contributes significantly to the increasing population

Table 3
Parameters used in the rate equation modeling.

Luminescence branching ratio and radiative and intrinsic (total) lifetimes of Ho^{3+}			
Transition (level#)	β[a]	τ_R[b]	τ (expt.)[c] (W_{NR} (s^{-1}[a])
$^5F_5$ (5) →		321 μs	16.3 μs (γ = 0) ($\tau_d = \tau$, W_{NR} (54) = 58234 s^{-1})
$^5I_5$ (4)	0.004		
$^5I_6$ (3)	0.046		
$^5I_7$ (2)	0.192		
$^5I_8$ (1)	0.758		
$^5I_5$ (4) →		6.8 ms	13 μs (γ = 350 $s^{-1/2}$) (τ_d = 135 μs, W_{NR} (43) = 7260 s^{-1}) (W_{CR} = 69231 s^{-1})
$^5I_6$ (3)	0.013		
$^5I_7$ (2)	0.430		
$^5I_8$ (1)	0.557		
$^5I_6$ (3) →		6.2 ms	4.8 ms (γ = 0) (W_{NR} (32) = 47 s^{-1})
$^5I_7$ (2)	0.058		
$^5I_8$ (1)	0.942		
$^5I_7$ (2) → $^5I_8$ (1)	1	16.2 ms	20.3 ms (γ = 0) (W_{NR} (21) = 0)
Energy transfer rate parameters (s^{-1}) (expt.)[d]			
HoF_3 (mol[a]%)	ETU_1 K_1 (s^{-1})	ETU_2 K_2 (s^{-1})	Cross-relaxation W_{CR} (s^{-1})
10%	8913	4221	69231

[a] Branching ratios calculated in this work.
[b] Radiative lifetimes calculated using Judd-Ofelt theory in this work.
[c] Experimental lifetime (intrinsic) obtained from the best fit to the luminescence done in this work.
[d] Experimental transfer rates obtained in this work.

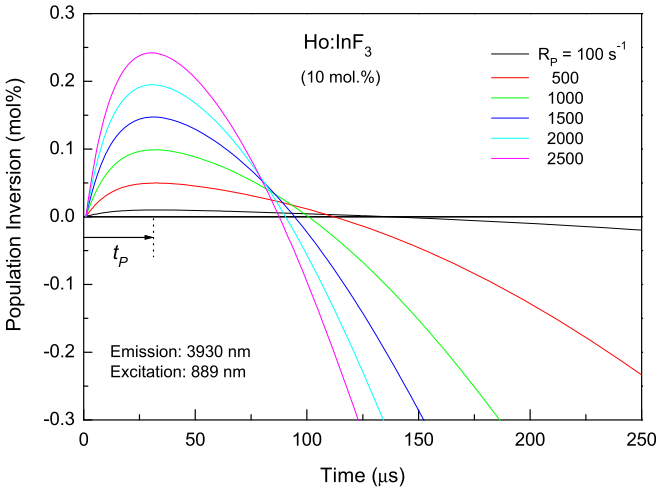

Fig. 15. Calculated population inversion (%) for the laser transition $^5I_5 \rightarrow {}^5I_6$ (at 3920 nm) as a function of the pump intensities for [Ho^{3+}] = 10 mol.% doped fluoroindate glass under CW pumping at 889 nm at 300 K. $R_P = 100$ s^{-1} corresponds to a pump intensity (I_P) equal to 51 kW cm^{-2}.

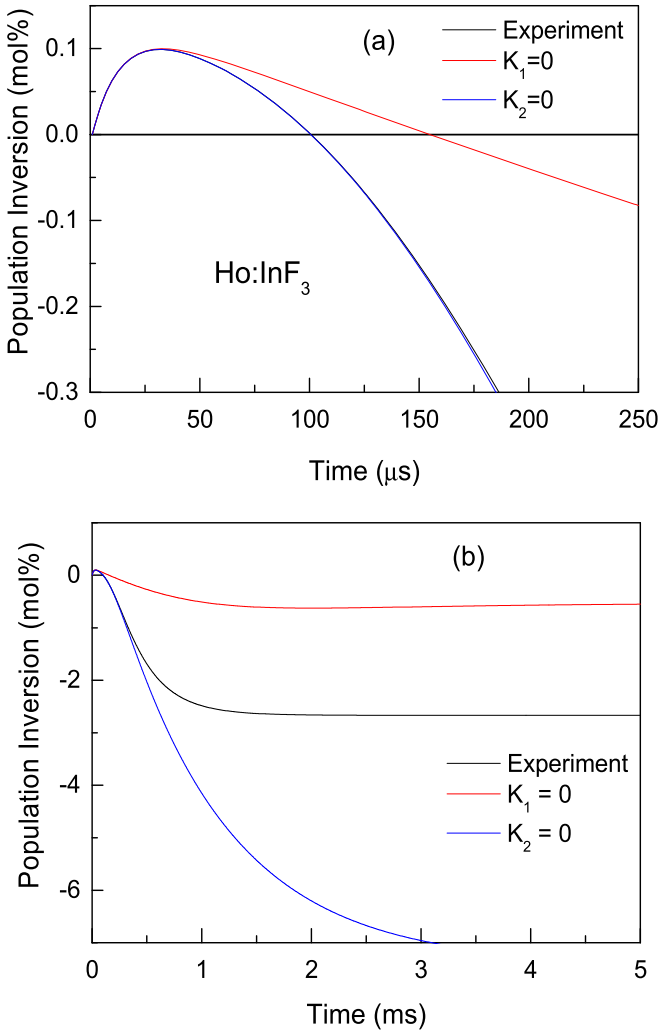

Fig. 16. Calculated population inversion for the laser transition $^5I_5 \rightarrow {}^5I_6$ (at 3920 nm) for CW pumping at 889 nm (at a rate $R_P = 1000\ s^{-1}$) for (a) a short time after initiating the pump and (b) up to 5 ms after the onset of optical pumping. The ETU rate parameters, K_1 and K_2 were either set equal to the measured values (black solid line), only the ETU_1 process is switched off ($K_1 = 0$) or only the ETU_2 process is switched off ($K_2 = 0$).

residing in the $^5I_6$ level (n_3), making the population inversion strongly negative. On the other hand, the ETU_2 process provides an increase to the population inversion. Overall, at the high Ho^{3+} concentration examined in this study, we can conclude that ETU is a significant problem and that future work should involve comprehensive spectroscopic studies involving a range of lower Ho^{3+} ion concentrations. Of course cascade lasing and co-doping with desensitizer ions may also assist with optimizing the emission from this transition.

5. Conclusions

The intrinsic luminescence efficiency of the $^5I_5 \rightarrow {}^5I_6$ transition with a peak wavelength of 3.92 μm in Ho^{3+}-doped fluoroindate glass was determined to be 0.33%; a value reduced from the radiative lifetime because of strong multiphonon emission and cross-relaxation processes. We observed that the decay time of the $^5I_6$ level in fluoroindate glass is close to the radiative lifetime because of the small multiphonon decay (of 47 s^{-1}). This result suggests this glass has no evidence of energy transfer to OH^- radicals. We measured the decay parameter for two well-known ETU processes involving the $^5I_7$ and $^5I_6$ excited states with the rates of these processes following the standard critical radius model which allowed the determination of the rate parameters. We established through rate equation modeling that at the 10 mol.% Ho^{3+}concentration used in this study, that the ETU processes severely limit laser emission at 3.92 μm and that a positive population inversion could only be obtained for relatively short $t_P < 100$ μs pump pulse durations.

Acknowledgments

The authors thank financial support from São Paulo State Research Foundation (FAPESP, Grants No 1995/4166-0 and 2000/10986-0), Brazilian Research Foundation (CNPq) and the Australian Research Council (DP140101336).

References

[1] J. Schneider, Electron. Lett. 31 (1995) 1250.
[2] J. Schneider, C. Carbonnier, U.B. Unrau, Appl. Opt. 36 (1997) 8595.
[3] A. Berrou, C. Kieleck, M. Eichhorn, Opt. Lett. 40 (2015) 1699.
[4] J. Gauthier, V. Fortin, J. Carrée, S. Poulain, M. Poulain, R. Vallée, M. Bernier, Opt. Lett. 41 (2016) 1756.
[5] V. Fortin, F. Maes, M. Bernier, S. Toubou Bah, M. D'Auteuil, R. Vallée, Opt. Lett. 41 (2016) 559.
[6] O. Henderson-Sapir, S.D. Jackson, D.J. Ottaway, Opt. Lett. 41 (2016) 1676.
[7] L. Nemec, J. Gotz, J. Am. Ceram. Soc. 53 (1970) 526.
[8] S.L. Oliveira, M.J.V. Bell, A. Florez, L.A.O. Nunes, J. Phys. D. Appl. Phys. 39 (2006) 3230.
[9] M.J. Weber, B.H. Matsinger, V.L. Donlan, G.T. Surratt, J. Chem. Phys. 57 (1) (1972) 562.
[10] T. Förster, Z. Naturforsch B 4a (1949) 321.
[11] A.I. Burshtein, Sov. JETP 35 (1972) 882.
[12] I. Bondar, A.I. Bursthein, A.V. Krutikov, L.P. Mesentseva, V.V. Osiko, V.P. Sakun, V.A. Smirnov, I.A. Shcherbakov, Sov. Phys. JETP 54 (1981) 45.
[13] A.M. Tkachuk, I.K. Razumova, E. Yu Perlin, M.F. Joubert, R. Moncorge, Opt. Spectrosc. 90 (1) (2001) 78.
[14] L.D. da Vila, L. Gomes, L.V.G. Tarelho, S.J.L. Ribeiro, Y. Messaddeq, J. Appl. Phys. 93 (2003) 3873.
[15] S.D. Jackson, A.F.H. Librantz, F.H. Jagosich, L. Gomes, G. Poirier, S.J.L. Ribeiro, Y. Messaddeq, J. Appl. Phys. 101 (2007) 123111.
[16] L. Gomes, F. Luty, Phys. Rev. B 30 (12) (1984) 7194.
[17] L. Gomes, A.F.H. Librantz, F.H. Jagosich, W.A.L. Alves, I.M. Ranieri, S.L. Baldochi, J. Appl. Phys. 106 (2009) 103508.
[18] L. Gomes, M. Oermann, H. Ebendorff-Heidepriem, D. Ottaway, T. Monro, A. Librantz, S.D. Jackson, J. Appl. Phys. 110 (2011) 083111.
[19] L. Gomes, D. Rhonehouse, D.T. Nguyen, J. Zong, A. Chavez-Pirson, S.D. Jackson, Opt. Mater. 50 (2015) 268.